

Metal Organic Frameworks

Preventing Undesirable Structure Flexibility in Pyromellitate Metal Organic Frameworks

Oliver G. Hayes,^[a] Stewart J. Warrender,^{*[a]} David B. Cordes,^[a] Morven J. Duncan,^[a] Alexandra M. Z. Slawin,^[a] and Russell E. Morris^[a]

Abstract: Removal of coordinated water molecules from the porous Zn-pyromellitate metal organic framework $Zn_5(OH)_2(PMA)_2(H_2O)_4 \cdot xH_2O$ (PMA = pyromellitic acid or 1,2,4,5-benzene tetracarboxylic acid) should generate coordinatively unsaturated metal sites suitable for gas adsorption. However, reports of instability towards dehydration have restricted the study and utility of this MOF. Here we examine in more detail the nature of the structural transformation that occurs upon dehydration. This study reveals that a fully reversible crystalline-

crystalline transformation from a porous to a non-porous homologue takes place, proceeding through a partially dehydrated intermediate. We show that doping the structure with Ni^{2+} ions at greater than 30 % prevents structural rearrangement, thereby maintaining porosity, and rendering the material effective for gas (nitric oxide) adsorption applications. These results indicate that doping can be an effective means to increase the utility of otherwise unserviceable structures.

Introduction

Metal organic frameworks (MOFs) offer unparalleled diversity amongst porous materials in terms of chemical composition, porosity and functionality. The vast and expanding variety of organic ligands and the multitude of coordination geometries offered by the pallet of metallic elements have permitted the development of highly tailorable novel materials with application-relevant properties. Consequently there is much promise of MOFs realising widespread research in fields as varied as CO_2 capture,^[1] fuel storage,^[2] gas separation,^[3] catalysis,^[4] sensors^[5] and drug delivery,^[6] to name a few, and there is continual efforts to seek and identify MOFs with improved and/or previously unobtainable functionality. Besides the variable and often tuneable nature of their composition, porosity and functionality, certain MOFs also exhibit the fascinating and potentially valuable phenomenon of structural flexibility. This feature is a result of the fundamental properties of the covalent, coordination and supramolecular bonds that underpin and define the structural geometry of MOFs. In addition to the rotation of bonds within ligands and between ligands and metal species, bond lability and supramolecular interactions can facilitate structural alteration. While many MOFs can be regarded as rigid and do not exhibit such structural flexibility, there are a grow-


ing number of flexible MOFs being developed for their unique adsorption properties and measurable physical changes brought about by external stimuli. Well known examples of flexible MOFs include MIL-47, MIL-53 and MIL-88, which form a group of materials that exhibit reversible “breathing” properties on exposure to simple guest species.^[7–10]

In contrast to “breathable” MOFs in which structural connectivity is maintained throughout the flexing process, there are many dynamic MOFs that exhibit complete or partial structural rearrangement upon exposure to a stimulating event. This group of MOFs includes so-called hemilabile MOFs that have been discussed extensively in a recent review.^[11] Such rearrangements can occur via crystalline-to-crystalline transformation, and in many cases the transformation is reversible. This is a very active branch of MOF development and is the subject of several reviews, which summarise many pertinent examples.^[12–14] Of particular relevance to the present study and the porous materials community is the phenomenon of reversible structural alteration upon dehydration/desolvation. Removal of solvent has been reported to induce either crystalline-crystalline or reversible amorphization structural transitions in some MOFs (see ref 14 for a review of key studies). There are a number of examples where such transformation can be beneficial; for example, for selective gas adsorption.^[15–18] However, dehydration-induced structural flexibility is not always desirable in the search for new functional materials where maintaining structure under multiple conditions is required (unexpectedly poor molecular sieving in ZIF-8 is one example^[19]). Since these properties are difficult to predict for a given MOF structure, the development of methods to control structure flexibility would greatly enhance functional capabilities of existing structures.

Many different methods by which to control structural flexibility have been reported.^[13,20] These include tuning particle

[a] O. G. Hayes, Dr. S. J. Warrender, Dr. D. B. Cordes, M. J. Duncan, Prof. A. M. Z. Slawin, Prof. R. E. Morris
University of St Andrews, School of Chemistry,
Purdie Building, North Haugh, St Andrews, Fife, Scotland, KY16 9ST, UK
E-mail: sjw9@st-andrews.ac.uk

 Supporting information and ORCID(s) from the author(s) for this article are available on the WWW under <https://doi.org/10.1002/ejic.202000322>.

 © 2020 The Authors. Published by Wiley-VCH Verlag GmbH & Co. KGaA. This is an open access article under the terms of the Creative Commons Attribution License, which permits use, distribution and reproduction in any medium, provided the original work is properly cited.

size,^[21] employing mixed ligand systems^[22] and post-synthetically exchanging^[23] or modifying ligands.^[24] It has also been shown that isostructures possessing different metal ions can exhibit contrasting flexibilities and adsorption properties.^[25–27] In addition, structural breathing can be fine-tuned by preparing heterometallic analogues that exhibit intermediate behaviour to those of the flexible monometallic counterparts.^[28] Such alteration in properties is possible due to the intrinsic differences in preferred coordination geometries, coordination numbers and bond lengths and strengths between one metal and another. It should be noted that the creation of heterometallic analogues is also an effective way to improve porosity,^[29] as well as to tune adsorption and release properties^[30] in rigid MOFs.

In the present study we investigate and report details of the transformations occurring upon dehydration in the pyromellitic acid (1,2,4,5-benzene tetracarboxylic acid, or “PMA”) based MOF $Zn_5(OH)_2(PMA)_2(H_2O)_4 \cdot xH_2O$ (hereafter referred to as **ZnPMA**). The synthesis and structure of this material (Figure 1a) was previously reported by Gutschke et al.^[31] Crucial features of its structure include elliptical channels measuring approximately 13 Å by 5 Å and the presence of pendant water molecules coordinated to some metal sites and protruding into the pore cavity, which if removed could form coordinatively unsaturated metal sites. However, despite possessing such key features relevant to gas adsorption application, Gutschke et al. reported that the structure is unstable to dehydration, forming an amorphous material. It therefore seemed unlikely that the material could be suitable for gas adsorption. Here we reveal that the dehydration-driven transformation is in fact a crystalline-crystalline transformation and that it can be prevented by doping the structure with Ni, thus rendering what was regarded as an un-serviceable MOF useful for gas adsorption and storage. The success of the approach is illustrated by employing the doped material as a delivery agent for the medically useful gas nitric oxide, and the study is expanded to confirm the generality of a previously disclosed approach of employing sequential doping to fine tune nitric oxide delivery.

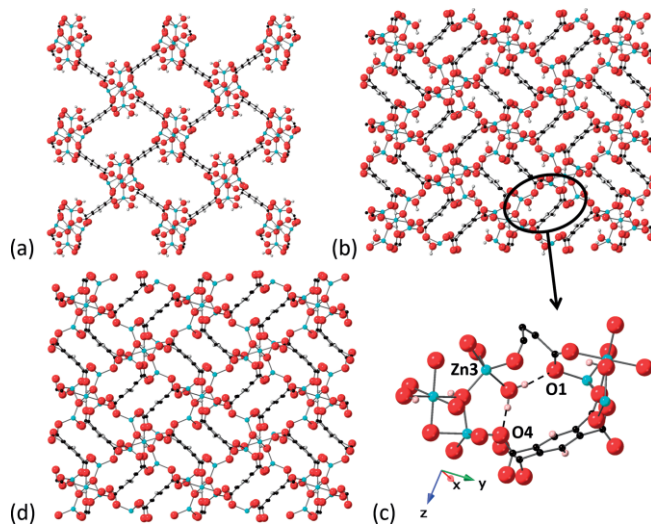


Figure 1. Framework structure of: **ZnPMA**, minus physisorbed pore water molecules, showing coordinated water molecules protruding into the one-dimensional pore channel (a), **ZnPMA-p**, showing change in porosity and retention of coordinated water molecules (b), detail of the cleft in which coordinated water molecules hydrogen-bond to framework oxygen atoms in **ZnPMA-p** (c), and **ZnPMA-d**, showing absence of coordinated water molecules (d). Figure (a), (b) and (d) are each viewed along the crystallographic x-axis; red – oxygen, cyan – zinc, black – carbon, grey – hydrogen.

Results and Discussion

Crystalline-Crystalline Transformation. Zn(II) acetate and PMA were reacted under both hydrothermal and reflux conditions (see Experimental Section). White crystalline material was obtained in each case; however, crystallites prepared via hydrothermal synthesis were larger than those obtained under reflux conditions. Powder x-ray diffraction (XRD) analysis (Figure S1) confirmed that the structure of both materials is that of the targeted phase $Zn_5(OH)_2PMA_2(H_2O)_4 \cdot xH_2O$ (**ZnPMA**). The structure can be considered to be constructed around $M_5(\mu_3-OH)_2$ “bow-tie” clusters in which two metal triangles share a common vertex (Figure 2a). The three crystallographically distinct metal

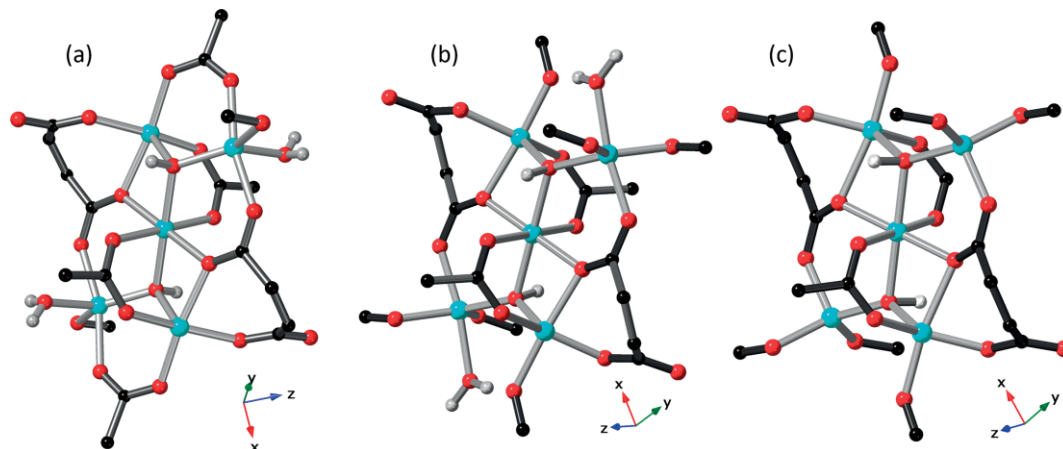


Figure 2. Comparison of the $M_5(\mu_3-OH)_2$ “bow-tie” units in **ZnPMA** (a), **ZnPMA-p** (b) and **ZnPMA-d** (c); red – oxygen, cyan – zinc, black – carbon, grey – hydrogen. Bonds shaded dark grey are internal to pyromellitate ligands.

atoms in each triangle exhibit different coordination environments (6- and 5-coordinate) and the ligand itself lacks any symmetry. The M_5 metal clusters are connected to adjacent clusters by four 1,1-carboxylate bridges to produce a structure with regular, one-dimensional channels, into which protrude coordinated water molecules. In accordance with the material's structural features and composition, a thermogravimetric analysis (TGA) profile (Figure 3a) broadly comprising two major mass losses was recorded; a mass loss of approximately 18 % at 100 °C representing loss of water, and a further loss of approximately 42 % above 380 °C representing decomposition of the organic ligand. Closer inspection also reveals a small reduction in mass of approximately 5 % around 200 °C.

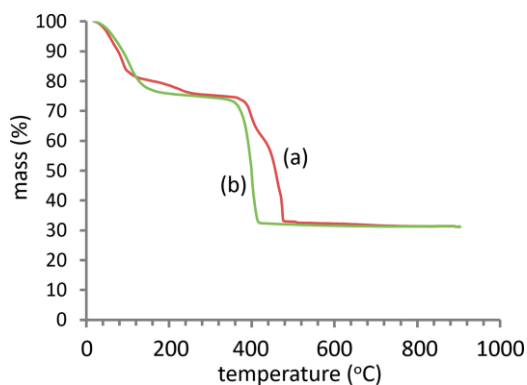


Figure 3. TGA profiles of **ZnPMA** (a) and **Ni/ZnPMA** (50:50 Ni:Zn) (b).

Variable temperature XRD (VTXRD) data were recorded in order to track the moment and progression of the previously reported but uncharacterised structural collapse on heating. Data were collected at 25, 60, 80, 100 and 120 °C to capture alterations associated with the first mass loss in the TGA profile, followed by collections at 150, 190, 220 and 260 °C to investigate any changes associated with the small inflexion at 200 °C. A final pattern was collected at 340 °C before allowing the sample to cool back to 25 °C. Figure 4 illustrates the resulting compilation of diffraction patterns and confirms a dramatic change in structure at 100 °C, and a further subtle alteration around 190 °C (most evident around 12–13° 2 θ). It is apparent that the

material does not lose long range order upon dehydration and, instead of becoming amorphous on dehydration as previously believed,^[31] undergoes a crystalline-crystalline transformation. The dehydrated structure remains stable up to at least 260 °C, but structural integrity is lost at 340 °C when the ligand decomposes. Data collected while the sample was cooling to room temperature (Figure 4b) suggest that the transformations observed to 340 °C are not reversible and the material remains amorphous, as would be expected following decomposition of the ligand. In a repeat of the experiment in which the sample was heated only to 190 °C (i.e. well below the onset temperature of structural loss) and cooled back to 25 °C (Figure S2), the changes in crystalline structure still appeared to be irreversible. However, powder XRD data collected from a dehydrated sample (heated to 170 °C) after sitting in ambient conditions for 24 hours (Figure 5a) reveal that the transformations are indeed reversible, but over a longer timescale than that employed in the VTXRD experiment.

The employed hydrothermal synthesis conditions permitted recovery of needle-shaped crystals suitable for single-crystal analysis. Given the slow kinetics of the rehydration process, it was postulated that conventional single-crystal analysis may be successful in capturing the dehydrated structure prior to reversion. A sample of **ZnPMA** was therefore dehydrated at 120 °C under a vacuum of 10^{-2} mbar, stored under dry argon and subsequently subjected to single-crystal X-ray analysis.

The structure of this thermally treated sample (Figure 1b, crystallographic data are summarised in Table 1) shows significant changes from that of the parent, most notably loss of porosity caused by a structural rearrangement. Indeed, BET measurements on the dehydrated phase yield a surface area of only 4 m²/g. Close inspection reveals that the $M_5(\mu_3\text{-OH})_2$ "bow-tie" units that constitute the hydrated form are still present and form the key structural backbone of the structure. However, the way in which they are connected has changed (Figure 2b); two 1,3-carboxylate bridges internal to the $M_5(\mu_3\text{-OH})_2$ units now bridge between adjacent units. A crucial and surprising feature is the remaining presence of coordinated water molecules on Zn3 indicating that the material has not been fully dehydrated, rather only the physisorbed water within the pore has been

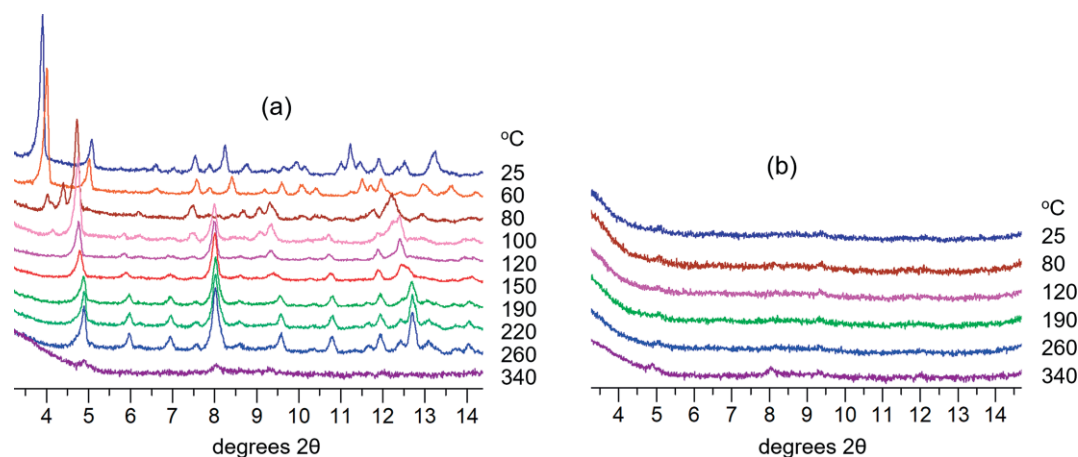


Figure 4. VTXRD data for **ZnPMA** collected during heating from 25–340 °C (a) and cooling from 340–25 °C (b). Data recorded using Mo $K_{\alpha 1,2}$ x-radiation.

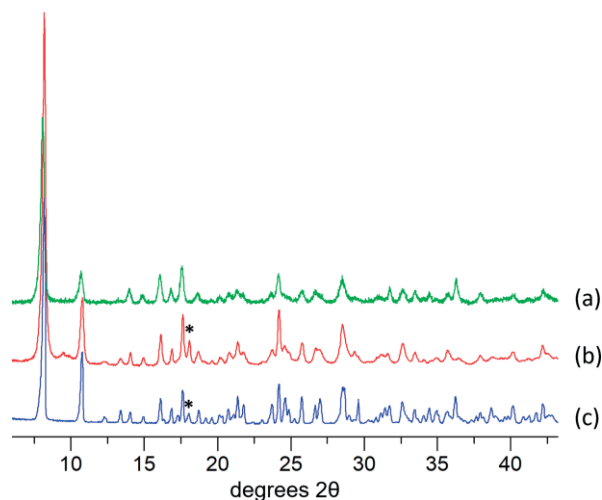


Figure 5. Powder XRD patterns of **ZnPMA** rehydrated under ambient conditions over 24 hours after being heated to 170 °C (a) and 250 °C (b), compared to a standard pattern (c) of as-made material. Note, pattern (a) was collected from the sample being loaded in a quartz capillary, and using a different diffractometer. *additional peak due to sample support. Data recorded using Cu $K_{\alpha 1}$ x-radiation.

removed. Accordingly, this structure is herein referred to as partially dehydrated **ZnPMA**, and denoted **ZnPMA-p**. Interestingly, the orientation of the coordinated water molecules has changed such that they protrude into a small cavity within the $M_5(\mu_3\text{-OH})_2$ chain (Figure 1c and Figure 2b), allowing for strong hydrogen bonding interactions with O1 and O4 [O–H...O distances 1.69(3) and 1.95(3) Å, O...O distances 2.661(7) and 2.930(7) Å]. **Figure S3** shows the close agreement between the powder XRD pattern recorded at 120 °C and that generated from the single-crystal structure, confirming that the solved structure is representative of the material at this temperature. Returning to the TGA analysis, the large mass loss at ca. 100 °C and the smaller loss at ca. 200 °C can now be fully rationalised; the loss of 18 % at ca. 100 °C corresponds closely to the reported quantity of physisorbed water (10 water molecules, 16 % of the formula unit mass) while the smaller mass loss of 5 % at ca. 200 °C corresponds to the quantity of coordinated water within the structure (4 molecules, 6 % of the formula unit mass), the loss of which can now be proposed as the reason for the subtle alterations observed above ca. 190 °C in the VT-XRD data.

In an attempt to capture the fully dehydrated structure (**ZnPMA-d**), the above experiment (whereby the sample was dehydrated and subjected to single-crystal analysis) was repeated but with the sample being heated to the higher temperature of 250 °C. Once again, the slow re-hydration kinetics permitted successful data collection and elucidation of the fully dehydrated structure. As anticipated, the fully dehydrated structure **ZnPMA-d** is isostructural to **ZnPMA-p**, but does not contain the coordinated water (Figure 1d and Figure 2c, Table 1). The subtle alterations in VT-XRD data that occur above 150 °C (Figure 4) are nicely corroborated by a comparison of theoretical powder XRD patterns for both **ZnPMA-p** and **ZnPMA-d** (**Figure S4**), generated from single-crystal data; for example, the shift in peaks at 4.8 and 5.8° 2θ to higher angle and the alterations between 12 and 13° 2θ.

Table 1. Selected crystallographic data.

	ZnPMA-p	ZnPMA-d
Empirical formula	$C_{20}H_{10}O_{20}Zn_5$	$C_{20}H_6O_{18}Zn_5$
fw	897.19	861.16
T [°C]	–148	–100
Crystal description	colourless needle	colourless needle
Crystal size [mm ³]	0.12 × 0.02 × 0.01	0.07 × 0.02 × 0.01
Space group	$P2_1/n$	$P2_1/n$
<i>a</i> [Å]	7.556(2)	7.7534(7)
<i>b</i> [Å]	14.333(4)	14.0219(14)
<i>c</i> [Å]	11.272(3)	11.0545(12)
β [°]	94.522(7)	95.628(10)
Vol [Å ³]	1217.0(6)	1196.0(2)
Z	2	2
ρ (calc) [g/cm ³]	2.448	2.391
μ [mm ^{–1}]	6.466	6.476
<i>F</i> (000)	880	840
Reflns collected	13088	11496
Independent reflns (<i>R</i> _{int})	2211 (0.0939)	2170 (0.1216)
Parameters/restraints	214/3	200/1
GOF on <i>F</i> ²	1.230	1.078
<i>R</i> ₁ [<i>I</i> > 2σ(<i>I</i>)]	0.0646	0.0642
<i>wR</i> ₂ (all data)	0.1768	0.1749
Largest diff. peak/hole [e/Å ³]	1.76, –0.57	1.06, –1.59

The powder X-ray diffraction pattern of **ZnPMA-d** after sitting in ambient conditions for 24 hours following heating at 250 °C compares very well to that of **ZnPMA**, with a slight broadening of peaks indicating some loss of crystallinity (note the peak at 18° 2θ is due to the sample support used in this case) (Figure 5b). It is therefore apparent that the structural rearrangements associated with both dehydration steps are completely reversible. Reversible alterations in the binding mode of carboxylate ligands is common in zinc complexes (and especially exemplified in enzymes) and is reported to proceed via a low energy pathway.^[32] The structural rearrangement is discussed further later. These results indicate that **ZnPMA** undergoes a crystalline-crystalline transformation on dehydration that involves the breaking and forming of coordinate bonds. As such, **ZnPMA** may be regarded as a further example of a hemilabile MOF.

Preventing Transformation

We have found that we can prevent this structural transformation occurring by partially replacing Zn²⁺ with Ni²⁺. When employing a 1:1 molar ratio of Zn and Ni acetate under the reflux synthesis conditions reported herein, a heterometallic polycrystalline analogue of the desired structure is obtained with approximate composition $Ni_{2.3}Zn_{2.7}(OH)_2(PMA)_2(H_2O)_4 \cdot xH_2O$ (referred to as **Ni/ZnPMA-50**; see elemental analysis **Table S1**, PXRD **Figure S5**). VT-XRD analysis indicates no dramatic structural rearrangement associated with the dehydration of this material (Figure 6). Indeed, BET analysis yields a surface area of 499 m²/g, suggestive of retained porosity. TGA analysis (Figure 3b) reveals a single dehydration step resulting in a 25 % mass loss. This corresponds to the combined quantities of pore and coordinated water in the structure and equals the sum of the two dehydration steps observed for **ZnPMA**. Since dehydration of **Ni/ZnPMA-50** does not lead to a structural transition, hydrogen

bonding between coordinated water and the framework (as observed in **ZnPMA-p**) cannot occur. This likely contributes to the reduction in temperature required to remove these water molecules compared to those in **ZnPMA-p**. As such, this stabilised material is very interesting from an applications viewpoint, and particularly for those applications which exploit coordinatively unsaturated metal sites, such as gas adsorption and storage.

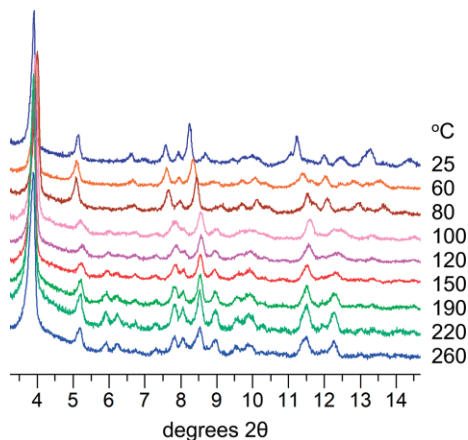


Figure 6. VT-XRD data for **Ni/ZnPMA-50** (50:50 Ni:Zn) collected during heating from 25–260 °C. Data recorded using Mo $K_{\alpha 1,2}$ X-radiation.

Utility of the Stabilised Structure

To probe the utility of the stabilised material and whether the anticipated coordinatively unsaturated metal sites are available for guest binding, **Ni/ZnPMA-50** was subjected to nitric oxide adsorption analysis. NO is a biological signaling molecule involved in many pathological and physiological processes and is of interest for medical applications.^[33] Results (Figure 7) indicate a dramatic improvement in performance compared to the zero uptake exhibited by the pure Zn analogue, with an adsorption of 3.9 mmol/g and storage of 2.5 mmol/g. Furthermore, the gas-loaded material exhibits good NO release performance, delivering 1.7 mmol/g over 2 hours (Figure 8e) under 11 % relative humidity. This indicates that the binding is reversible, and that release can be triggered by moisture in a fashion akin to the likes of CPO-27 MOFs. Although efficiency of delivery vs. storage is lower for **Ni/ZnPMA-50** than for CPO-27 MOFs, the quantity of NO released is still sufficient to elicit a biological response.^[30]

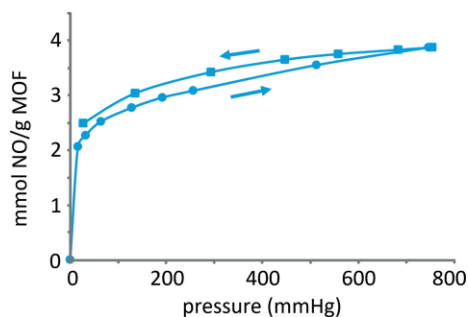


Figure 7. Gravimetric NO adsorption/desorption isotherms for **Ni/ZnPMA-50** (50:50 Zn:Ni).

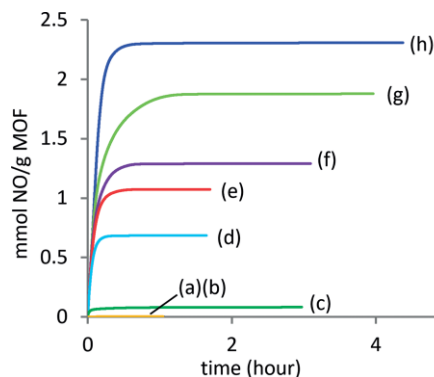


Figure 8. Total NO release under 11 % relative humidity from Ni-doped ZnPMA materials **Ni/ZnPMA-10** (a), **Ni/ZnPMA-20** (b), **Ni/ZnPMA-30** (c), **Ni/ZnPMA-40** (d), **Ni/ZnPMA-50** (e), **Ni/ZnPMA-60** (f), **Ni/ZnPMA-70** (g), **Ni/ZnPMA-80** (h) and **Ni/ZnPMA-90** (i).

The stabilisation of the structure using only 50 % Ni²⁺ present in the synthesis and the realisation that heterometallic analogues could be prepared raised the questions: (1) how little dopant is necessary to stabilise the structure, and (2) would sequential doping result in tuneable NO delivery in a similar manner to doped Mg/Ni-CPO-27.^[30] A series of Ni-doped materials were therefore prepared under reflux conditions with compositions ranging from 10–100 mol-% Ni. Surprisingly, reaction mixtures containing 100 mol-% Ni did not yield the Ni analogue of the desired structure, despite indications from Gutschke et al. that isostructural analogues could be formed (both Zn and Co analogues were reported by Gutschke). Instead, when using 100 % Ni, an as yet unreported structure was obtained. The reasons for this are not yet clear and require further analysis. The structure and properties of this **NiPMA** material will be discussed elsewhere. **Table S1** lists compositional analysis results for samples prepared from reaction mixtures containing 10–90 % Ni. The data indicate close correlation between targeted and obtained compositions. Powder XRD data shown in **Figure S5** indicate that samples containing up to 60 % Ni possess the **ZnPMA** structure. Beyond this level, subtle differences in the XRD pattern compared to **ZnPMA** suggest that slight structural variation may be induced by the higher Ni content, however the structure does not dramatically change until zinc is entirely removed from the synthesis, suggesting a possible structure directing influence of Zn. NO release experiments (Figure 8) reveal a dependency of delivered NO levels on Ni substitution, as has been shown and explained previously for Ni-doped Mg-CPO-27.^[30] This permits tuning of the delivered NO dose, which is essential when seeking to selectively trigger the many possible biological responses to NO (such as vasodilation, anti-thrombus, angiogenesis and antimicrobial efficacy to name a few^[33]). Closer inspection reveals that NO release is negligible at Ni levels of 10 and 20 % and a marked step-change in release occurs between 30 and 40 % Ni. VT-XRD analysis of a 10 % Ni sample (**Figure S6**) indicates that at such levels the structure still exhibits dehydration-driven structural rearrangement. Unexpectedly, VT-XRD analysis of the 30 % Ni sample reveals that the dehydrated sample likely contains a mixture of both the stabilised and rearranged structures (**Figure S7**). SEM imaging

indicates two morphologies are present in this sample (rod-shaped crystals and clusters of smaller more irregularly shaped crystals). EDX analysis suggests that Ni and Zn are present in both morphologies but possibly in slightly different ratios; the rod-shaped crystals having approximately 17–21 % Ni, while the smaller crystals have 23–29 % Ni (Figures S8 and S9). This variation may be further evidence to suggest that approximately 30 % Ni marks a transition point in thermal stability. Although materials doped with greater than 50 % Ni show subtle alterations in the base structure, as evidenced by powder XRD (Figure S5), they appear to exhibit good thermal stability, as exemplified in the VT-XRD analysis of a sample doped with 80 % Ni (Figure S10). Indeed, NO release continues to increase at these high levels of doping, indicative of structure retention. It is therefore considered that at least 30 % (and preferably 40 %) Ni is required in order to stabilise the **ZnPMA** structure and render it useful for gas adsorption/release.

Rearrangement and Stabilisation Pathways

It is evident from the results of this study that Ni plays a direct role in preventing the structural rearrangement. It is difficult at this stage to ascertain the precise mechanism of the rearrangement and stabilisation, particularly without evidence of the location of Ni²⁺ in the structure. Here we suggest some possible explanations, which would require validation through further investigation.

The octahedral site at the centre of the structural bow-tie unit remains little changed after the transformation and could be regarded as not playing a key role in the rearrangement. This site represents 20 % of all metal sites in the unit cell. We observe that structural rearrangement is only prevented after 20 % of metal sites are doped with Ni²⁺, therefore it may be logical to propose Ni²⁺ preferentially occupies this octahedral site at doping levels of 10 and 20 %. (Note CFSE is greater for octahedral d⁸ compared to trigonal bipyramidal d⁸ and octahedral d¹⁰). This may be a possible explanation for the lack of influence exerted by Ni levels below 30 %. We postulate that at levels greater than 20 %, Ni begins to occupy 5-coordinate positions including the site to which water is bound. It is apparent that this site undergoes the most dramatic alteration during the rearrangement and appears to be most critical to the process. This may be a reason why Ni levels greater than 20 % have a more dramatic effect on stability. We do not as yet have data that indicates a reason why the occupancy of this site by Ni should favour retention of original structure; however geometric preferences (e.g. for 4 and 6 coordination) and the flexibility of L–M–L bond angles could be important.

In the case of **ZnPMA**, d¹⁰ Zn²⁺ shows a general ambivalence towards coordination geometry and can accept a wider range of geometries more readily than d⁸ Ni²⁺. In this situation the ability of Zn to participate in highly exchangeable ligand binding may be important. It is possible that energy contributions from the cleavage and formation of Zn–PMA bonds, in addition to the stabilisation gained through hydrogen bonding following rearrangement, favour the initial retention of 5-coordinate geometry and reorganisation of the structure to **ZnPMA-p**

(note hydrogen bonding is a well-known contributing factor in many structural rearrangements^[34]). This is in preference to the direct formation of the dehydrated 4-coordinate environment despite Zn's ability to adopt 4-coordinate geometry. It could also be the case that direct dehydration of the **ZnPMA** structure might result in an unfavourably strained 4 coordinate geometry, possibly constrained by the presence of the 1,3-carboxylate bridging moiety, which could restrict framework flexibility. However, release of the bridging group during dehydration of **ZnPMA** and formation of **ZnPMA-p**, may afford a less strained and more favourable 4-coordinate Zn environment. By whatever mechanism, the structural rearrangement of **ZnPMA** upon removal of physisorbed pore water molecules appears to provide a lower energy pathway than complete dehydration and retention of original structure.

Conclusion

This study has shown that **ZnPMA** undergoes a crystalline-crystalline transformation on dehydration rather than amorphization as previously believed. We have shown that heterometallic doping with Ni²⁺ is an effective strategy for preventing this undesirable structural flexibility and that the material can be rendered highly useful as a delivery agent for the medically relevant gas nitric oxide (and potentially more widely for gas storage in general). Our study has shown that, in the search for new and improved functionality, revisiting seemingly unserviceable flexible MOFs may yield new opportunities.

Experimental Section

All reagents were commercially available and used without further purification. PMA and Zn(II) acetate dihydrate were purchased from Aldrich, Ni(II) acetate tetrahydrate was purchased from Acros, while NaOH solution was purchased from Fluka.

Hydrothermal synthesis of mono-metallic materials. PMA (0.382 g, 1.5 mmol) was dissolved in NaOH solution (0.55 M, 11 mL) at room temperature whilst stirring. Zinc acetate (1.5 mmol) was dissolved in distilled water (5 mL) at room temperature whilst stirring. Once both the PMA and metal salt were dissolved, the PMA solution was added to the Teflon liner of a 30 mL capacity autoclave followed by the metal salt solution. The autoclave was heated at 175 °C for 24 hours. Once removed from the oven, the autoclave was cooled to room temperature before the product was recovered by filtration, washed with water (10 mL) and allowed to dry overnight under ambient conditions.

Reflux synthesis of mono- and hetero-metallic materials. PMA (0.382 g, 1.5 mmol) was dissolved in NaOH solution (0.55 M, 11 mL), whilst stirring, and heated to 65 °C. The appropriate metal salt (zinc or nickel acetate, 1.5 mmol) or mixtures of zinc and nickel acetate in the desired molar ratio (totalling 1.5 mmol, see Table S1) was dissolved in distilled water (5 mL) at room temperature whilst stirring. Once fully dissolved, the metal salt solution was added swiftly to the PMA solution whilst stirring. This mixture was heated under reflux for 24 hours. After cooling to room temperature, the mixture was filtered and washed with water (10 mL). The powder product was dried overnight in ambient conditions.

Powder X-ray diffraction (XRD) data collection was conducted using a PANalytical Empyrean diffractometer employing CuK_{α1} radiation

monochromated with a curved Ge (111) crystal in reflectance mode. Variable temperature powder X-ray diffraction (VTXRD) data were collected using a PANalytical Empyrean diffractometer employing Mo $K_{\alpha 1,2}$ radiation. Samples were heated at 5°/min to strategic temperatures identified from thermogravimetric analysis. Data were collected over one hour after a dwell time of 30 min at temperature. Selected samples, where indicated, were analysed in transmission mode (quartz glass capillary sample holders) using a STOE STADIP diffractometer employing $CuK_{\alpha 1}$ radiation monochromated with a curved Ge (111) crystal.

Partially dehydrated **ZnPMA**, referred to as **ZnPMA-p**, was prepared by heating at 120 °C under a vacuum of 10^{-2} mbar for 2 hours. Fully dehydrated **ZnPMA**, referred to as **ZnPMA-d**, was prepared by heating to 250 °C under a vacuum of 10^{-2} mbar for 2 hours. Both samples were stored under dry argon prior to analysis.

Single-crystal X-ray diffraction data for partially dehydrated and fully dehydrated ZnPMA (referred to as **ZnPMA-p** and **ZnPMA-d**, respectively) were collected at low temperature (−148 °C or −100 °C) using a Rigaku MM-007HF High Brilliance RA generator/confocal optics with either an XtaLAB P200 or XtaLAB P100 diffractometer [$Cu K_{\alpha}$ radiation ($\lambda = 1.54187 \text{ \AA}$)]. Intensity data were collected using either ω steps or both ω and φ steps accumulating area detector images spanning at least a hemisphere of reciprocal space. Data for all compounds analysed were collected and processed (including correction for Lorentz, polarization and absorption) using CrystalClear^[35] or CrysAlisPro.^[36] Structures were solved by direct methods (SIR2004)^[37] and refined by full-matrix least-squares against F^2 (SHELXL-2018/3).^[38] Non-hydrogen atoms were refined anisotropically, and aromatic hydrogen atoms were refined using a riding model. Hydroxyl and water hydrogen atoms were located from the difference Fourier map and refined isotropically subject to a distance restraint, and with thermal motion riding on the parent oxygen atom for **ZnPMA-p**. All calculations were performed using the CrystalStructure^[39] interface. Selected crystallographic data are presented in Table 1.

Deposition Number(s) CCDC 1938658 and 1938659 contain(s) the supplementary crystallographic data for this paper. These data are provided free of charge by the joint Cambridge Crystallographic Data Centre and Fachinformationszentrum Karlsruhe Access Structures service www.ccdc.cam.ac.uk/structures.

Thermogravimetric analysis (TGA) was performed using a Netzsch TGA 209 instrument, in which the sample (ca. 5 mg) was heated to 900 °C at a rate of 5 °C/min in air. BET measurements were carried out at −196 °C using a Micromeritics ASAP 2020 surface area and porosity analyser. Samples were prepared by removal of solvent by heating to 150 °C at a ramp rate of 10 °C/min under vacuum for 1000 minutes. Nitrogen gas was then incrementally dosed onto the sample and the volume of gas adsorbed was measured as a function of partial pressure. Thermodynamic nitric oxide adsorption/release isotherms were measured gravimetrically using bespoke apparatus, and kinetic release measurements were recorded using a Sievers NOA 280i chemiluminescence nitric oxide analyser under flowing humid nitrogen (11 % relative humidity), both as described previously^[40] and described in SI. ICP-MS was conducted using an Agilent 7500 series ICP-MS spectrometer with appropriate calibration standards ranging from 0.1–20 ppm, and all analyses conducted in triplicate. EDX analysis was conducted on a JEOL 5600 SEM electron microscope in both mapping and single point analysis modes.

Acknowledgments

This project has received funding from: the European Union's Horizon 2020 research and innovation program under grant agreement No 685727; the Engineering & Physical Sciences Research Council (EPSRC) under awards EP/K005499/1 and EP/K039210/1; and the University of St Andrews School of Chemistry.

Keywords: Crystalline-crystalline transformation · Doping · Metal-organic frameworks · Nitric oxide · Structure elucidation

- [1] C. A. Trickett, A. Helal, B. A. Al-Maythaly, Z. H. Yamani, K. E. Cordova, O. M. Yaghi, *Nat. Rev. Mater.* **2017**, *2*, 17045.
- [2] Y. He, F. Chen, B. Li, G. Qian, W. Zhou, B. Chen, *Coord. Chem. Rev.* **2018**, *373*, 167.
- [3] H. Li, K. Wang, Y. Sun, C. T. Lollar, J. Li, H.-C. Zhou, *Mater. Today* **2018**, *21*, 108.
- [4] A. Dhakshinamoorthy, Z. Li, H. Garcia, *Chem. Soc. Rev.* **2018**, *47*, 8134.
- [5] A. Chidambaram, K. C. Stylianou, *Inorg. Chem. Front.* **2018**, *5*, 979.
- [6] M.-X. Wu, Y.-W. Yang, *Adv. Mater.* **2017**, *29*, 1606134.
- [7] K. Barthelet, J. Marrot, D. Riou, G. Ferey, *Angew. Chem. Int. Ed.* **2002**, *41*, 281.
- [8] C. Serre, F. Millange, C. Thouvenot, M. Nogues, G. Marsolier, D. Louer, G. Ferey, *J. Am. Chem. Soc.* **2002**, *124*, 13519.
- [9] N. A. Ramsahye, G. Maurin, S. Bourrelly, P. L. Llewellyn, T. Loiseau, C. Serre, G. Ferey, *Chem. Commun.* **2007**, *31*, 3261.
- [10] C. Serre, C. Mellot-Draznieks, S. Surble, N. Audebrand, Y. Filinchuk, G. Ferey, *Science* **2007**, *315*, 1828.
- [11] R. E. Morris, L. Brammer, *Chem. Soc. Rev.* **2017**, *46*, 5444.
- [12] K. Uemura, R. Matsudo, S. Kitagawa, *J. Solid State Chem.* **2005**, *178*, 2420.
- [13] J.-P. Zhang, H.-L. Zhou, D.-D. Zhou, P.-Q. Liao, X.-M. Chen, *Natl. Sci. Rev.* **2018**, *5*, 907.
- [14] A. Halder, D. Ghoshal, *CrystEngComm* **2018**, *20*, 1322.
- [15] E. Jeong, W. R. Lee, D. W. Ryu, Y. Kim, W. J. Phang, E. K. Koh, C. S. Hong, *Chem. Commun.* **2013**, *49*, 2329.
- [16] a) P. K. Allan, B. Xiao, S. J. Teat, J. W. Knight, R. E. Morris, *J. Am. Chem. Soc.* **2010**, *132*, 3605; b) B. Xiao, P. J. Byrne, P. S. Wheatley, D. S. Wragg, X. Zhao, A. J. Fletcher, K. M. Thomas, L. Peters, J. S. O. Evans, J. E. Warren, W. Zhou, R. E. Morris, *Nat. Chem.* **2009**, *1*, 289.
- [17] A. Halder, B. Bhattacharya, R. Dey, D. K. Maity, D. Ghoshal, *Cryst. Growth Des.* **2016**, *16*, 4783.
- [18] J. Arinez-Soriano, J. Albalad, C. Vila-Parrondo, J. Perez-Carvajal, S. Rodriguez-Hermida, A. Cabeza, J. Juanhuix, I. Imaz, D. MasPOCH, *Chem. Commun.* **2016**, *52*, 7229.
- [19] H. Bux, F. Liang, Y. Li, J. Cravillon, M. Wiebcke, J. Caro, *J. Am. Chem. Soc.* **2009**, *131*, 16000.
- [20] S. K. Elsaidi, M. H. Mohamed, D. Banerjee, P. K. Thallapally, *Coord. Chem. Rev.* **2018**, *358*, 125.
- [21] O. M. Linder-Patton, W. M. Bloch, C. J. Coghlan, K. Sumida, S. Kitagawa, S. Furukawa, C. J. Doonan, C. J. Sumbly, *CrystEngComm* **2016**, *18*, 4172.
- [22] I. Schwedler, S. Henke, M. T. Wharmby, S. R. Bajpe, A. K. Cheetham, R. A. Fischer, *Dalton Trans.* **2016**, *45*, 4230.
- [23] C.-X. Chen, Z. Wei, J.-J. Jiang, Y.-Z. Fan, S.-P. Zheng, C.-C. Cao, Y.-H. Li, D. Fenske, C.-Y. Su, *Angew. Chem. Int. Ed.* **2016**, *55*, 9932.
- [24] Z. Wang, S. M. Cohen, *Am. Chem. Soc.* **2009**, *131*, 16675.
- [25] F. Millange, N. Guillou, R. I. Walton, J.-M. Greneche, I. Margiolaki, G. Ferey, *Chem. Commun.* **2008**, 4732.
- [26] a) J. A. Mason, J. Oktawiec, M. K. Taylor, M. R. Hudson, J. Rodriguez, J. E. Bachman, M. I. Gonzalez, A. Cervellino, A. Guagliardi, C. M. Brown, P. L. Llewellyn, N. Masciocchi, J. R. Long, *Nature* **2015**, *527*, 357; b) H. J. Choi, M. Dinca, A. Dailly, J. R. Long, *Energy Environ. Sci.* **2010**, *3*, 117.
- [27] M. Sadakiyo, T. Yamada, K. Kato, M. Takata, H. Kitagawa, *Chem. Sci.* **2016**, *7*, 1349.
- [28] a) F. Nour, T. Devic, H. Chevreau, N. Guillou, E. Gibson, G. Clet, M. Daturi, A. Vimont, J. M. Greneche, M. I. Breeze, R. I. Walton, P. L. Llewellyn, C.

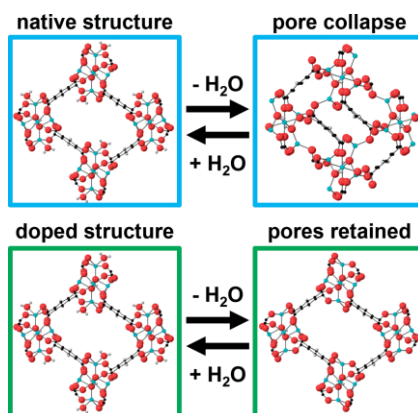
- Serre, *Chem. Commun.* **2012**, 48, 10237; b) M. I. Breeze, G. Clet, B. C. Campo, A. Vimont, M. Daturi, J. M. Greneche, A. J. Dent, F. Millange, R. I. Walton, *Inorg. Chem.* **2013**, 52, 8171.
- [29] J. Kahr, R. E. Morris, P. A. Wright, *CrystEngComm* **2013**, 15, 9779.
- [30] D. Cattaneo, S. J. Warrender, M. J. Duncan, C. J. Kelsall, M. K. Doherty, P. D. Whitfield, I. L. Megson, R. E. Morris, *RSC Adv.* **2016**, 6, 14059.
- [31] S. O. H. Gutschke, D. J. Price, A. K. Powell, P. T. Wood, *Eur. J. Inorg. Chem.* **2001**, 2739.
- [32] M. A. Gil, W. Maringgele, S. Dechert, F. Meyer, *Z. Anorg. Allg. Chem.* **2007**, 633, 2178.
- [33] A. Butler, R. Nicholson, *Life, Death and Nitric Oxide*, Royal Society of Chemistry, Cambridge, **2003**.
- [34] S. Kitagawa, K. Uemura, *Chem. Soc. Rev.* **2005**, 34, 109.
- [35] *CrystalClear-SM Expert* v2.1. Rigaku Americas, The Woodlands, Texas, USA, and Rigaku Corporation, Tokyo, Japan, **2015**.
- [36] *CrysAlisPro* v1.171.38.46. Rigaku Oxford Diffraction, Rigaku Corporation, Oxford, U. K. **2015**.
- [37] M. C. Burla, R. Caliandro, M. Camalli, B. Carrozzini, G. L. Cascarano, L. De Caro, C. Giacovazzo, G. Polidori, R. Spagna, *J. Appl. Crystallogr.* **2005**, 38, 381.
- [38] G. M. Sheldrick, *Acta Crystallogr., Sect. C* **2015**, 71, 3.
- [39] *CrystalStructure* v4.3.0. Rigaku Americas, The Woodlands, Texas, USA, and Rigaku Corporation, Tokyo, Japan, **2018**.
- [40] D. Cattaneo, S. J. Warrender, M. J. Duncan, R. Castledine, N. Parkinson, I. Haley, R. E. Morris, *Dalton Trans.* **2016**, 45, 618.

Received: April 1, 2020

Metal Organic Frameworks

O. G. Hayes, S. J. Warrender,*
D. B. Cordes, M. J. Duncan,
A. M. Z. Slawin, R. E. Morris 1–9

Preventing Undesirable Structure Flexibility in Pyromellitate Metal Organic Frameworks



Doping of a Zn-pyromellitic acid-based metal organic framework with Ni prevents a detrimental, reversible, crystalline-crystalline transformation occurring on dehydration and permits delivery of the medically useful gas nitric oxide from the previously un-serviceable material.

0

doi.org/10.1002/ejic.202000322